3 Experiment

The experimental set-up can technically be split in two parts: the laser system, which provides the laser pulses, and the ultra-high vacuum (UHV) chamber, which houses the sample, the equipment for sample preparation, the energy analyzer and the spin-polarization detector. While the laser set-up will just be introduced briefly the UHV chamber will be discussed in detail. Finally, a description of sample preparation will be given owing to its importance in growth of epitaxial thin films.

3.1 Set-up

3.1.1 Laser system

The laser pulses are provided by a home-build Ti:sapphire laser, which is pumped by a Nd:YVO_4 laser. It runs at a repetition rate of 88 MHz and delivers Gaussian-shaped pulses with a width of 40 fs. Its wavelength is tunable between 765 nm and 840 nm and an average power of about 850 mW - 920 mW is achieved. The pulses are split in two parts, 30% are used for the probe pulse and 70% for the pump pulse. To excite the image-potential states, a photon energy close to the work function of the sample is necessary (typically 4.6 eV - 4.8 eV in this experiment). This is obtained by frequency doubling the laser fundamental in a Lithium Triborat (LBO) crystal and a subsequent sum-frequency generation with the remaining part of the fundamental pulse in a Beta Barium Borat (BBO) crystal. The resulting frequency-tripled pump pulse is aligned in time and space to the probe pulse and focused on the sample. The glancing angle of incidence forms an elliptical-shaped spot with an area which is estimated to about $4 \cdot 10^{-4}$ cm^2. To achieve a variable time delay between the pulses, the probe pulse passes a delay stage. The cross correlation of the two pulses is obtained by two-photon photoemission of the occupied Shockley surface state on Cu(111) via a virtual intermediate state. Beside the pulse width of the pump-pulse the cross correlation also delivers the point of zero time delay between the pulses. The polarization of the laser pulses can be set by a $\lambda/2$-wave plate to either p-polarization or s-polarization. The fundamental laser pulse can be characterized with a spectrometer and an autocorrelator. Table 3.1 summarizes all important parameters of the pump and

	pump pulse	probe pulse
wavelength (nm)	255 - 280	765 - 840
photon energy (eV)	4.86 - 4.42	1.62 - 1.48
pulse width (fs)	55	40
power (mW)	5 - 12	185 - 210

Table 3.1: *Parameters of pump and probe pulses used for 2PPE in the present experiment. The maximum power is obtained at the central wavelength of the oscillator at 795 nm. Note that the pump-pulse and probe-pulse photon-energy is related by frequency tripling.*

probe pulses. More details about the laser set-up will be presented in [*Schmidt*, 2007].

3.1.2 UHV chamber

The UHV chamber consists of two parts, a preparation and an analysis chamber. Due to the high reactivity of ferromagnetic metal surfaces and the sensitivity in film growth to residual gases, an ultra-high vacuum is a prerequisite in this experiment. A base pressure below $4 \cdot 10^{-11}$ mbar has been achieved in both chambers by the use of standard pumping techniques. The separation of these two parts with a gate valve provides the possibility to keep ultra-high vacuum in the analysis chamber during sample cleaning in the preparation chamber or vice versa during flashing of the W(100) crystal of the spin-polarization detector. The sample can be transferred on a manipulator between the two chambers. A pressure rise to $5 \cdot 10^{-10}$ mbar was encountered during sample transfer, which usually took about 2 minutes.

As illustrated in Figure 3.1 the preparation chamber bears:

- Sputter gun for sample cleaning
- Quadrupole mass spectrometer for residual and sputter gas analysis
- Cobalt and iron evaporators based on electron bombardment heating (EFM-3, Focus GmbH). The cobalt evaporator is placed normal to the surface to preclude a steering induced magnetization anisotropy [*van Dijken et al.*, 1999]. The iron evaporator is oriented with 30° to the sample normal.
- Quartz microbalance for calibration of the evaporators
- Electron gun for MEED. Angle of incidence of the electron beam is 80° with respect to the surface normal
- LEED optics, LEED screen is also used for MEED

The components in the analysis chamber (see Figure 3.1) are:

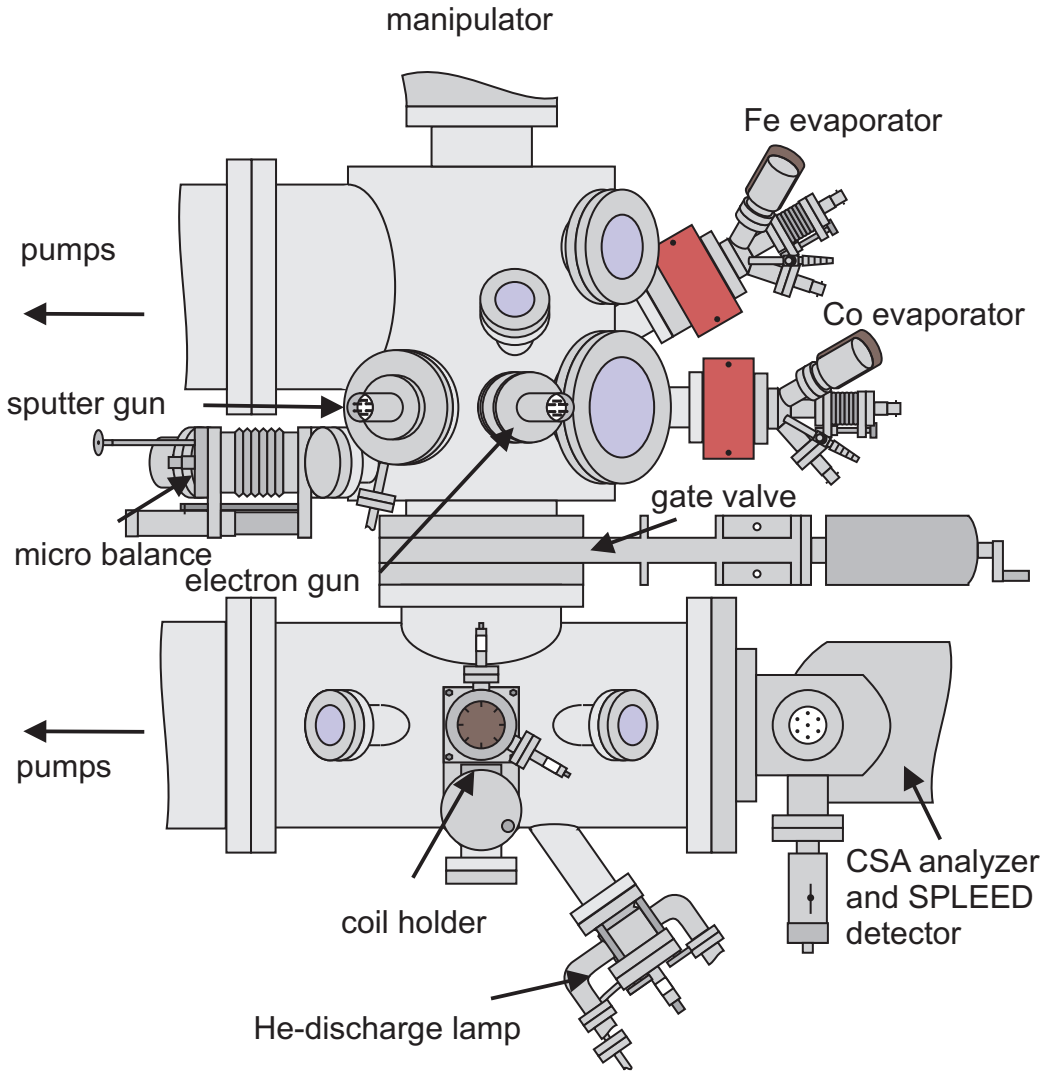

Figure 3.1: *Overview of preparation chamber (upper part) and of analysis chamber (lower part). The LEED optics and the quadrupole mass spectrometer cannot be seen in this side view as well as the two entrance windows for the laser beam.*

- Two entrance windows, which are made out of fused silica to have a high transmission for UV light. They allow an incidence angle of 80° and 45° with respect to the sample normal for the incoming laser pulses.

- He-discharge lamp emitting He I radiation (21.2 eV), used for analyzer performance tests

- Coil with 10 windings to magnetize the sample. The attachment to a z-transfer with xy-tilt provides an exact positioning and a complete retraction from the sampling area. Additionally, it is rotatable around its axis to magnetize the sample either *in-plane* or *out-of-plane*. A remanent magnetization is obtained by applying a current pulse on the coil. The maximum magnetic field strength at the sample position is estimated to be about 200 Oe.

- Cylindric sector analyzer with spin-polarization detector (see corresponding sections).

- μ-metal shielding to keep away magnetic stray fields from the analyzing area. This is necessary due to the low kinetic energy of the photoemitted electrons and the torque of a magnetic field on the spin. The magnetic field inside the analysis chamber was determined to be smaller than 2 mG. The reduction of any stray field was an additional reason for choosing ultrathin ferromagnetic films as samples and not bulk ferromagnets.

Electron analyzer

The experiments were performed with a cylindric sector field analyzer (CSA 300, Focus GmbH) in combination with a spin-polarization detector (see next paragraph). A CSA was chosen because of its high transmission and a 90° deflection of the electrons within the analyzer. The latter allows for a spin-polarization detection in both, an *in-plane* and an *out-of-plane* magnetization direction of the sample (see also Figure 3.5). The analyzer has a transfer-lens system which is designed for a 50 mm working distance to the sample and was especially optimized for low-energy electrons. It decelerates or accelerates the electrons to adapt their kinetic energy to the appropriate pass energy E_{pass} of the cylindric sector analyzer. The pass energy defines the kinetic energy of the electrons which are transmitted in the analyzer. This constant pass-energy mode ensures a constant energy resolution throughout the whole energy range. The transmission was found to vary less than 10 % in the significant energy range of this experiment at a sample bias of 1.5 V.

The aperture at the entrance lens defines the angular resolution of ±5°. The energy resolution $\Delta E/E_{pass}$ generally depends on the beam width in the dispersive direction given by the size of the slits w_1, w_2 and on the semiangular apertures

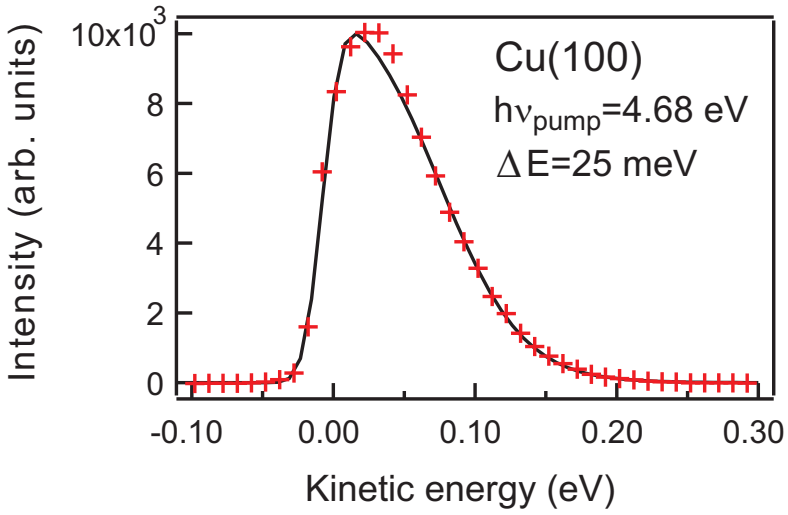

Figure 3.2: *Low-energy cut-off of Cu(100) measured with a pump-pulse photon energy of 4.68 eV. For the simulation (solid line) an analyzer resolution of 25 meV was used.*

in the dispersive (α) and non-dispersive directions (β) [*Roy and Carette*, 1977]. The overall resolution is therefore given by:

$$\frac{\Delta E}{E_{pass}} = \frac{1}{4}A(w_1 + w_2) + \frac{1}{4}B\alpha^n + \frac{1}{4}C\beta^2. \tag{3.1}$$

For this analyzer the coefficients are $A = 2/D$, $B\alpha^n = 0.003$, $C\beta^2 = 0.035$, where D denotes the distance between entrance and exit slit and is 300 mm. For typical experimental conditions ($E_{pass} = 1$ eV and $w_1 + w_2 = 4$ mm) we get a resolution of $\Delta E = 25$ meV full width at half maximum. This value could be verified by measuring the broadening of the low-energy cut-off of Cu(100) as shown in Figure 3.2. The low-energy cut-off stems from electrons at the Fermi level E_F which are directly excited with the pump pulse. The prerequisite for this is a photon energy $h\nu_p$ which equals or is larger than the sample work-function ϕ. The simulation in Figure 3.2 is therefore based on convolution of a Gaussian function, which represents the analyzer resolution ΔE with a Fermi distribution, which is cut off below $E_F - (h\nu_p - \phi)$. Precisely, a slight broadening of the Fermi distribution due to the spectral width of the pump pulse ΔE_p has also been considered. In total the simulation is given by:

$$I(E) \propto \left(\Theta\left(E + h\nu_p - \phi\right) \cdot \left(\frac{1}{\exp(\frac{E}{k_bT}) + 1} \otimes \exp(-4\ln 2\frac{E^2}{\Delta E_p})\right)\right) \otimes \exp\left(-4\ln 2\frac{E^2}{\Delta E}\right) \tag{3.2}$$

However, in most measurements an inhomogeneous broadening was present, which led to a resolution of about 50 meV. In combination with the spectral width of the probe pulse of about 40 meV an overall resolution of 70 meV was obtained, which could be verified by linewidth measurements on Cu(100).

Spin-polarization detector

The spin-polarization detection is based on spin-polarized low energy electron diffraction (SPLEED) [*Kirschner and Feder*, 1979]. The schematic drawing in Figure 3.3 illustrates its principle. An incident electron beam with a defined energy (here: 104.5 eV) impinges normal to a tungsten (100) surface. Two pairs of channeltrons are placed in the (20),($\bar{2}$0) and (02),(0$\bar{2}$) diffraction beams, respectively. The spin-dependent scattering potential causes a left-right asymmetry in the spin polarization of the respective diffraction beams. In case of an already polarized incoming electron beam, this transfers to an asymmetry in the intensity. Vice versa one can deduce the spin polarization P from the respective difference in count rates. So far assuming an equal channeltron counting efficiency the spin polarization P is determined by

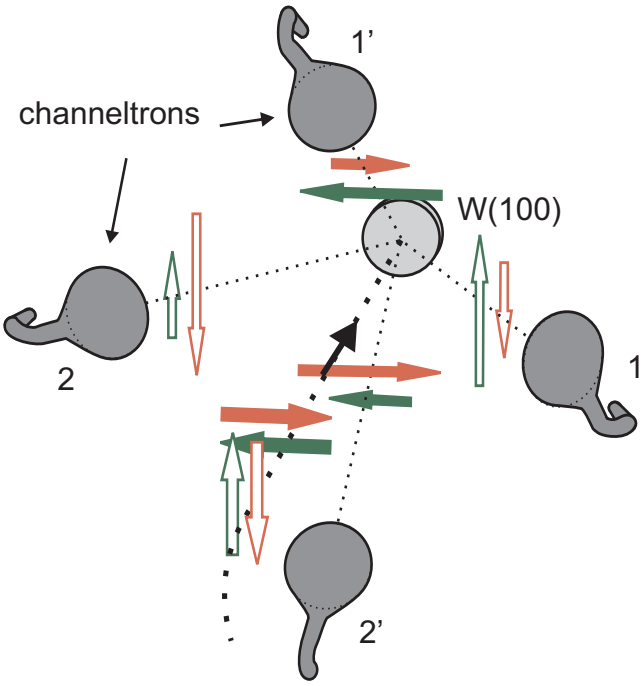

Figure 3.3: *Schematic of the working principle of a SPLEED detector. The filled and unfilled arrows denote the spin-polarization vectors for the two accessible directions. Their length in the diffracted beams indicate the change in spin polarization.*

$$P = \frac{1}{S}\frac{N_1 - N_2}{N_1 + N_2} \tag{3.3}$$

whereas S is the Sherman function, which corresponds to the asymmetry of a 100% spin-polarized beam and N_1 and N_2 are the respective count rates in the channeltrons. The problem of an initial counting asymmetry, which would lead to an erroneous determination of the spin polarization, can be bypassed by two ways: The easiest possibility is to record a spectrum with antiparallel spin-polarization of the photoelectrons, which is usually achieved by reversing the magnetization direction. The spin polarization can thus be evaluated by taking the geometric mean value of the respective count rates of both measurements A and B.

$$P = \frac{1}{S}\frac{\sqrt{N_{1A}N_{2B}} - \sqrt{N_{2A}N_{1B}}}{\sqrt{N_{1A}N_{2B}} + \sqrt{N_{2A}N_{1B}}} \tag{3.4}$$

The spin-up and spin-down count rate is given by

$$I_\uparrow = \frac{1+P}{2}(N_1 + N_2) \tag{3.5}$$

$$I_\downarrow = \frac{1-P}{2}(N_1 + N_2) \tag{3.6}$$

or in the case of being able to reverse the spin polarization of the photoelectrons by taking the sum of the geometric mean value of both measurements as in equation 3.4. This, however, requires a certain symmetric arrangement of the set-up. As discussed later in section 4.3 the two magnetization directions may spectroscopically be inequivalent for an *in-plane* magnetization. Therefore data obtained for opposite magnetization directions must not be compared. To deduce the spin polarization and consider the initial asymmetry one has in this case to normalize N_1 in equation 3.3 and 3.5 by the ratio of the channeltron count rates measured with an unpolarized electron beam of $R = N_1^0/N_2^0$.

The crucial parameters of an experiment are the Sherman function S and the detector related count-rate asymmetry which is defined in this work by the ratio R [1]. For the Sherman function only a lower boundary of $S = 0.23$ could be determined, which was also used for data evaluation. As an upper boundary one may use the theoretical predicted value of $S = 0.33$ [*Kirschner and Feder*, 1979]. A detailed discussion about the determination of the Sherman function and the initial count-rate asymmetry is given in the Appendix A.

Throughout one day of measurements no significant change in S was observed, which dispensed with the necessity of cleaning the W(100) crystal between the

[1] It can also be defined as $R' = \frac{N_1^0 - N_2^0}{N_1^0 + N_2^0}$ [*Kirschner and Feder*, 1979]

measurements. The ratio of the channeltron count rates R was ranging from 1 to 1.4. During one day the change was small (less than 1 % in one hour) but a larger shift between several days was observed, especially due to thermal movements of the W(100) crystal during cleaning procedures. At this point one has to note that the channeltron count rates and therefore also R are very sensitive to the electron beam path and incidence angle on the tungsten crystal. Even small modifications in the geometrical arrangement close to the sample, e.g. moving a coil below it, lead to a change in R.

The price one has to pay for the spin resolution is a huge loss in count rate which is about three orders of magnitude [*Kirschner*, 1985a]. A larger transmission of the analyzer and a larger power of the pump and probe pulses compared to standard 2PPE experiments could compensate this effect considerably and count rates have been achieved in the range of 10000 counts per second (cps) for the n=1 image-potential state.

The error of a possible wrong assignment of the Sherman function S and detector related asymmetry R is taken into account for the values of the binding energy but not for the error bar of the individual data points in the spectra. This error bar is based on the statistical error as described in the Appendix B.

More details about the SPLEED detector can be found in [*Kirschner*, 1985a,b] or more generally about spin-polarized electrons in [*Kessler*, 1985].

Sample holder

As displayed in Figure 3.4 the sample holder bears two crystals: Cu(111) for reference measurements and Cu(100) as a substrate for the ferromagnetic thin films. The requirement for the sample holder is to allow for a variable temperature range between 90 and 900 K. The cooling is achieved by a coldfinger which itself is cooled by a liquid nitrogen basin, provided by the pipe shape of the upper part of the manipulator head. A good thermal but electric insulating contact to the specific sample mounts is ensured via sapphire plates. The Cu(111) crystal can be heated by applying a current through the tantalum wires which hold the crystal. A current of usually 11 A was necessary to heat the crystal up to 800 K. The Cu(100) crystal can be heated with electron bombardment from two filaments behind the sample. These two filaments also provide radiation assisted heating, which was used for temperature regulation during temperature-dependent measurements. An antiparallel arrangement of the filaments suppresses magnetic fields at the sample during operation, which would severely influence the trajectories of the photoexcited electrons and thus also the count rate during the measurements. Only a relative change of 10% in 2PPE intensity has been observed by applying of a filament current of 1.3 A, which is necessary to heat the crystal to about

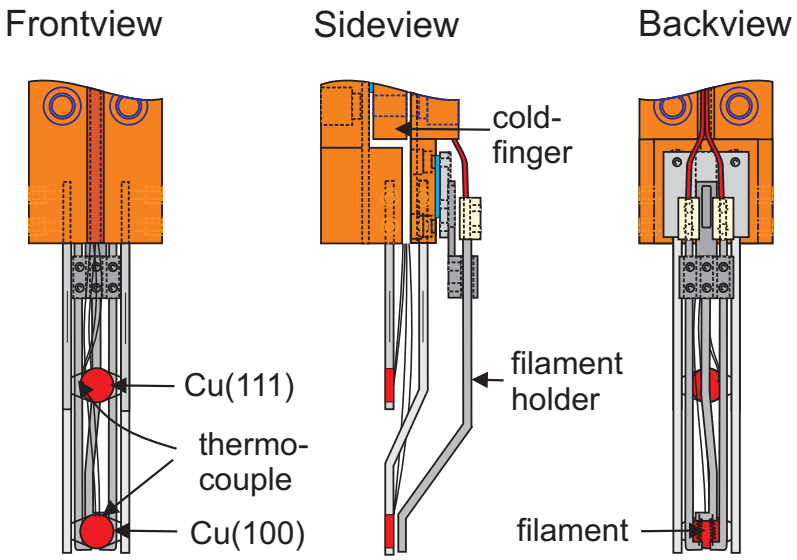

Figure 3.4: *Three different views on the sample holder.*

300 K. Due to its low Curie temperature and high temperature sensitivity a type E (NiCr/CuNi) thermocouple is used for temperature reading[2].

Measurement geometry

The schematic drawing in Figure 3.5 summarizes the geometric arrangement of the components described above, including the sample position and the incoming laser pulses. The entrance window which offers an incidence angle of 80° to the surface normal provides a smaller focal spot and a higher degree of p-polarization and thus a larger count rate compared to the other window at an angle of 45° and was therefore chosen for all measurements. With the rotatable coil the sample can be magnetized either *in-plane* or *out-of-plane* with respect to the sample surface. The deflection of the electrons by 90° in the energy analyzer allows for a spin sensitivity in these two directions since the longitudinal spin component, which corresponds to the *out-of-plane* direction, is converted into a transversal one and can therefore be measured with a SPLEED detector. This leads to a high flexibility in the choice of ferromagnetic samples.

3.2 Sample preparation

A clean and flat substrate is necessary for a good quality of the film. To check for sample cleanness and smoothness, 2PPE of image-potential states was employed.

[2]The sample holder was initially designed for tungsten crystals. Only a change of the thermocouple would be necessary to change to this system.

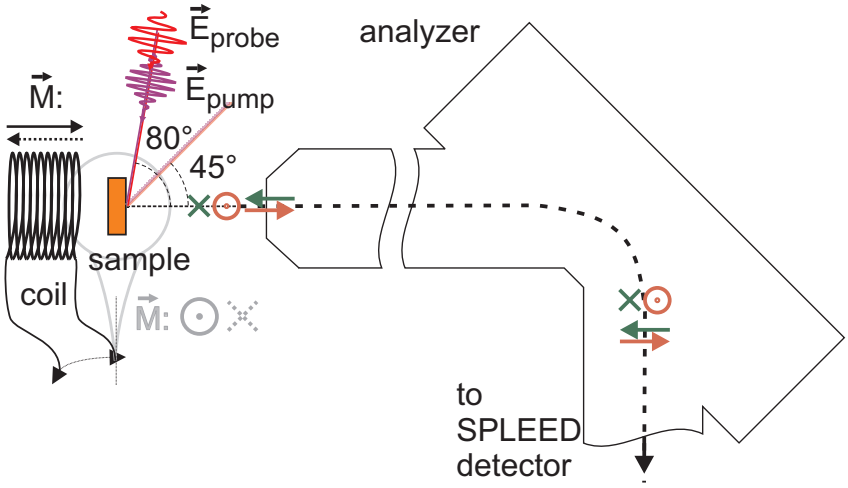

Figure 3.5: *Schematic of the measurement geometry of the experiment. The coil can be rotated to magnetize the sample either out-of-plane (↑↓) or in-plane (× ⊙) with respect to the sample surface.*

Long lifetimes and low dephasing rates are a reliable indication for a flat and defect free surface [*Boger*, 2004]. It turned out that usually 5 minutes of argon sputtering with an energy of 800 eV and a subsequent annealing to 700 K for 6 minutes is adequate.

The films were deposited with a rate of 0.5 ML/min at room temperature and, in the case of cobalt, also at 100 K. In the latter case the film was annealed afterwards to 470 K for 10 minutes. Measurements of the lifetime, and the binding energy of image-potential states as a function of annealing temperature for a 5 ML Co/Cu(100) film suggested no significant change in the film structure, i.e. no Cu diffusion on top of the film [*Schmid et al.*, 1993]. The room temperature grown films were not annealed with the exception of a slight annealing to 340 K of the 7 ML iron film used for the temperature-dependent measurement in section 5.2.

During growth MEED was employed as a tool for an exact film thickness characterization with a typical error of 0.2 ML, whereas the quartz microbalance was just taken for calibration after bakeout or a change of evaporator settings. Beside the determination of the film thickness MEED curves can also be used to study the growth mode. A layer-by-layer growth mode of ultrathin Co and Fe films on Cu(100) grown at room temperature could well be observed, except for the first two monolayers, which is in accordance to literature [*Kief and Egelhoff*, 1993]. For the growth of Co at 90 K, the growth mode is three dimensional, which almost results in a complete loss of any oscillations in the MEED pattern. In this case the Co evaporator had to be calibrated regularly, e.g. by growth on Cu(100) at room temperature. Therefore an error in coverage of 10% had to be encoun-

tered. We could not observe any significant changes neither in the exchange splitting nor the spin polarization of the image-potential states throughout the whole time of data acquisition, which usually lasted up to 8 hours. We took this as an indication for clean and stable conditions for the measurements.

The tungsten crystal had been flashed to 2300 K before a series of measurements was taken to remove tungsten-oxide. Flashes between measurements were redundant due to the stable conditions as verified by a constant exchange splitting and spin polarization of the studied systems over time. After measuring the tungsten crystal was passivated with oxygen to prevent any reaction of the clean W(100) crystal with residual gases. About once a week and after bakeout several cycles of annealing at an oxygen partial pressure of $5 \cdot 10^{-8}$ mbar and flashes to 2300 K were performed. This procedure leads to a depletion of carbon contamination in the near-surface region.

3.3 Measurement procedure

After the sample had been cleaned and the laser power had been optimized, the zero point of the delay between the pump and probe pulse was deduced. This was done by 2PPE from the occupied Shockley surface state on Cu(111). A perfectly overlapping pump and probe pulse yields a maximum in intensity, which can be adjusted by a time-resolved measurement.

The spin-resolved measurements were always recorded in both magnetization directions. For *out-of-plane* magnetized samples this has the advantage to exclude experimental artifacts like a detector-related asymmetry as described in Section 3.1.2. The energy-resolved spectrum was always recorded completely in one magnetization direction and subsequently in the opposite direction. By assigning the letter A to the measurement in one magnetization direction and B to the one in opposite direction the measurement sequence for a multiple number of scans was

$$ABAB...AB.$$

For the *in-plane* magnetized cobalt films the change of the magnetization direction allowed us to study of dichroic effects (see Chapter 4.3). However, the detector-related asymmetry has to be determined separately (see Appendix A). Since a decrease of the laser power or the detection efficiency between the measurements in both magnetization directions can pretend dichroism the following sequence for the measurements in both magnetization directions (A and B) was chosen:

$$ABBAABBA...ABBA.$$

This sequence cancels any effects due to a linear decrease of the laser power or detection efficiency in time.

In contrast to the energy-resolved measurements the magnetization direction in time-resolved measurements was always changed at every delay step. The integration time per data point (10 - 30 s) was long enough to let the capacitors in the magnetization power supply recharge and short enough to neglect any decrease in laser power. This had also the advantage of an exactly equivalent zero point of the time delay between the measurements in opposite magnetization direction.